Scattered acoustic field above a grating of non-parallel rectangular cavities

Adel Khanfir, Adil Faiz, Joël Ducourneau, J. Chatillon, Salaheddine Skali-Lami

Scattered acoustic field above a grating of non parallel rectangular cavities

A. Khanfir[a], A. Faiz[b], J. Ducourneau[b], J. Chatillon[c], S. Skali Lami[b]

[a] *Laboratoire dAcoustique de l'Université du Maine (LAUM), Université du Maine. Av. Olivier Messiaen, 72085, Le Mans Cedex 9, France.*
[b] *Laboratoire d'Énergétique et de Mécanique Théorique et Appliquée, Université de Lorraine, 2, avenue de la Forêt de Haye, BP160, 54504 Vandoeuvre-lès-Nancy Cedex, France.*
[c] *Institut national de recherche et sécurité (INRS), Rue du Morvan CS 60027 54519 Vandoeuvre-lès-Nancy Cedex France.*

Abstract

Geometric or acoustical irregularities induces acoustic scattering. In this paper, a generalization of the model proposed by Khanfir et al (Journal of Sound and Vibration, 332 (4), 2013) to determine the scattered acoustic field above gratings of parallel rectangular cavities is developed, addressing the case of gratings of non parallel rectangular cavities. The results provided by the model were compared both to numerical results, obtained with the finite element method, and to experimental ones. The observed agreement between the analytical predictions and the numerical and experimental results supports the validity of the proposed model. The coupling between the different cavities was investigated, in order to attain an explanation for its dependence on frequency and on the spacing between cavities.

Keywords: scattered acoustic field, rectangular cavity, coupling phenomena

1. Introduction

The problem of acoustic wave scattering by gratings of parallel rectangular cavities has been extensively studied by many authors. Holford [1]

Email addresses: adel.khanfir@gmail.com (A. Khanfir), jacques.chatillon@inrs.fr (J. Chatillon)

represents the reflected field above a periodic wall facing by an infinite sum of plane waves. De Bruijn [2], Ando et al. [3] and Ducourneau et al. [4] use the waveguide model to study periodic gratings of rectangular cavities. Park et al. [5] applied a trigonometric series-based representation of the diffracted field to investigate electromagnetic scattering from multiple rectangular apertures in a thick conducting screen. Hongo et al. [6, 7] use the Kobayashi Potential method to study diffraction of electromagnetic waves by arrays of thin parallel slits and arrays of thin parallel plate waveguides respectively. Khanfir et al [8] use the Kobayashi Potential (KP) method to study diffration of acoustic waves by an aperiodic grating of parallel rectangular cavities.

The solution presented in this paper is a generalization of the model developed by Khanfir et al [8] to the case of gratings containing non parallel rectangular cavities. This model allows mastering the scattering behavior of gratings of rectangular cavities. Thus, it will be possible to plot directivity diagrams of the reflected acoustic field and thus to estimate an acoustic diffusion coefficient. This parameter can be then used to acoustically characterize such a wall facings. It can also be used in predictive softwares to predict the soundscape in industries (RayPlus software for example [9]).

2. Statement of the problem

Let us consider N rectangular cavities in a thick, rigid, large screen. The cavities edges are perfectly rigid. We assume that a uniform incident plane wave $\Phi_{\text{inc}}^{\text{pl}}$ impringes on the N rectangular cavities with a perfectly rigid edges in an infinitely rigid screen, as shown in figure 1. Let η_{ad}^{i} be the characteristic admittance of the bottom of the ith cavity. θ_i is the angle between the ith local frame (O, x_i, y_i, z) and the reference frame (O, x, y, z). The ith cavity dimensions are $2a_i$, $2b_i$ and d_i respectively in the directions x_i, y_i and z.

Each cavity, defined by the region of space $D_i = \{(x, y) \,/\, |x_i| < a_i,\, |y_i| < b_i\} \subset \mathbb{R}^2$, contains a modal field Φ_{w}^{i}. The total acoustic field above the grating consists of :

- the incident field $\Phi_{\text{inc}}^{\text{pl}}$,
- the specular reflected field Φ_r,
- the diffracted field composed by a superposition of the elementary diffracted fields Φ_{d}^{i} generated by each cavity.

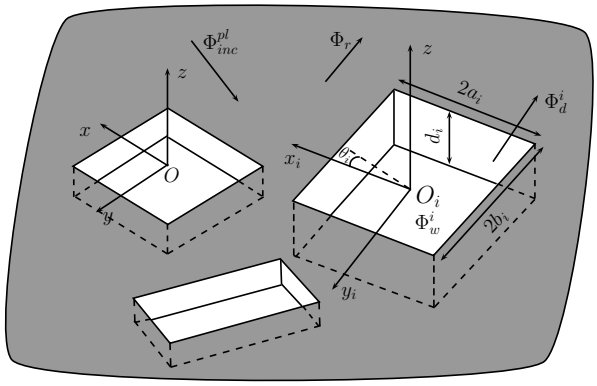

Figure 1: Geometry of the studied wall facing and the different acoustic fields.

The expressions of the different fields are given by Khanfir et al [8]:

$$\Phi_{\text{inc}}^{\text{pl}} = Ae^{\text{j}k_x x}e^{\text{j}k_y y}e^{\text{j}k_z z} \tag{1}$$

$$\Phi_{\text{r}} = Ae^{\text{j}k_x x}e^{\text{j}k_y y}e^{-\text{j}k_z z} \tag{2}$$

$$\Phi_{\text{w}}^i = \sum_{p\geq 0}\sum_{q\geq 0}\cos\left(\frac{p\pi}{2}(\xi_i+1)\right)\cos\left(\frac{q\pi}{2}(\eta_i+1)\right)\left[E_{pq}^i e^{-\gamma_{pq}^i\frac{z}{a_i}} + F_{pq}^i e^{\gamma_{pq}^i\frac{z}{a_i}}\right] \tag{3}$$

$$\Phi_{\text{d}}^i = \sum_{m,n\geq 0}\iint_{\mathbb{R}_+^2}\frac{A_{mn}^i\Phi_{cc}^{(m,n)^i} + B_{mn}^i\Phi_{cs}^{(m,n)^i} + C_{mn}^i\Phi_{sc}^{(m,n)^i} + D_{mn}^i\Phi_{ss}^{(m,n)^i}}{e^{\frac{z}{a_i}\sqrt{\alpha^2+(\frac{a_i}{b_i}\beta)^2-(ka_i)^2}}}\text{d}\alpha\,\text{d}\beta \tag{4}$$

where $\mathbf{k} = \begin{pmatrix} k_x \\ k_y \\ k_z \end{pmatrix}$ is the incident wave vector, $\xi_i = \frac{x_i}{a_i}$, $\eta_i = \frac{y_i}{b_i}$, α and β are

integration variables and:

$$\gamma_{p,q}^{i} = \sqrt{(\frac{p\pi}{2})^2 + (\frac{a_i}{b_i}\frac{q\pi}{2})^2 - (ka_i)^2} \tag{5}$$

$$\Phi_{cc}^{(m,n)^i} = \frac{J_{2m}(\alpha)J_{2n}(\beta)}{\sqrt{\alpha^2 + (\frac{a_i}{b_i}\beta)^2 - (ka_i)^2}}\cos(\alpha\xi_i)\cos(\beta\eta_i) \tag{6}$$

$$\Phi_{cs}^{(m,n)^i} = \frac{J_{2m}(\alpha)J_{2n+1}(\beta)}{\sqrt{\alpha^2 + (\frac{a_i}{b_i}\beta)^2 - (ka_i)^2}}\cos(\alpha\xi_i)\sin(\beta\eta_i) \tag{7}$$

$$\Phi_{sc}^{(m,n)^i} = \frac{J_{2m+1}(\alpha)J_{2n}(\beta)}{\sqrt{\alpha^2 + (\frac{a_i}{b_i}\beta)^2 - (ka_i)^2}}\sin(\alpha\xi_i)\cos(\beta\eta_i) \tag{8}$$

$$\Phi_{ss}^{(m,n)^i} = \frac{J_{2m+1}(\alpha)J_{2n+1}(\beta)}{\sqrt{\alpha^2 + (\frac{a_i}{b_i}\beta)^2 - (ka_i)^2}}\sin(\alpha\xi_i)\sin(\beta\eta_i) \tag{9}$$

A is the amplitude of the incident field. The amplitude of the specular reflected field is equal to the amplitude of the incident field due to the rigidity of the surface separating the cavities ($R = 1$). A_{mn}^i, B_{mn}^i, C_{mn}^i, D_{mn}^i, E_{pq}^i and F_{pq}^i are unknown modal amplitudes determined by enforcing the boundary conditions : continuity of acoustic pressure and velocity and a mixed boundary condition at the ith cavity bottom. This different boundary conditions are respectively given by relationships (10)-(12). The purpose is to determine the diffracted fields Φ_{d}^i. Thus, the modal amplitudes A_{mn}^i, B_{mn}^i, C_{mn}^i, D_{mn}^i are the main unknowns to determine.

$$\frac{\partial}{\partial z}\left(\Phi_{\mathrm{inc}}^{\mathrm{pl}} + \Phi_{\mathrm{r}} + \Phi_{\mathrm{d}}^i + \sum_{j\neq i}\Phi_{\mathrm{d}}^j\right) = \frac{\partial}{\partial z}\Phi_{\mathrm{w}}^i,\ (x_i, y_i) \in D_i,\ z = 0,\ 1 \leq i \leq N \tag{10}$$

$$\Phi_{\mathrm{inc}}^{\mathrm{pl}} + \Phi_{\mathrm{r}} + \Phi_{\mathrm{d}}^i + \sum_{j\neq i}\Phi_{\mathrm{d}}^j = \Phi_{\mathrm{w}}^i,\ (x_i, y_i) \in D_i,\ z = 0,\ 1 \leq i \leq N \tag{11}$$

$$\frac{\partial \Phi_{\mathrm{w}}^i}{\partial z} - \mathrm{j}k\eta_{\mathrm{ad}}^i\Phi_{\mathrm{w}}^i = 0,\ (x_i, y_i) \in D_i,\ z = -d_i,\ 1 \leq i \leq N \tag{12}$$

Relationships between the local frames and the reference frame are not given by a simple translation such as the case of parallel the cavities [8]. They are given by a combination of a rotation and a translation (see figure 2) as shown in equations (13)-(15):

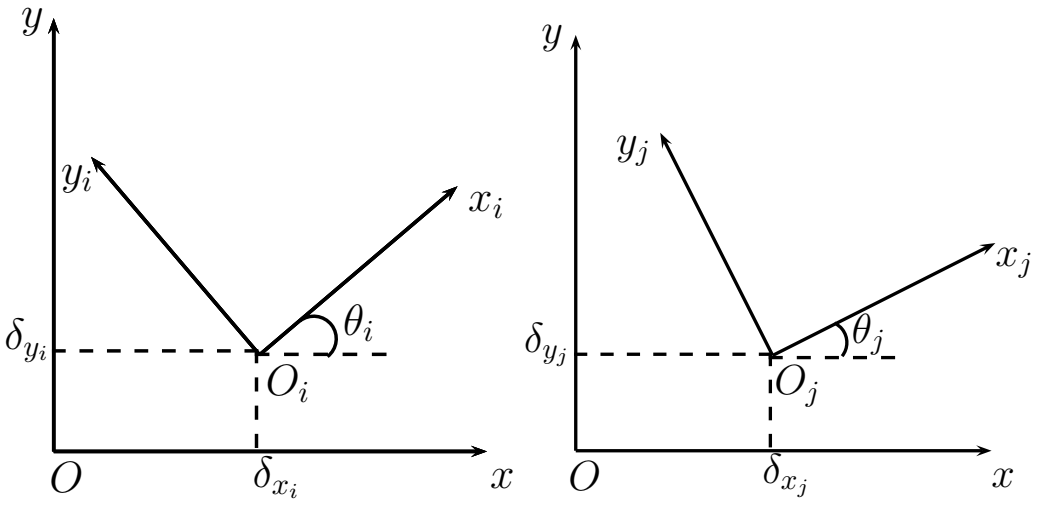

Figure 2: Position of the local frame (O_i, x_i, y_i) (a) and the the local frame (O_j, x_j, y_j) (b) in the reference frame (O, x, y)

$$\begin{pmatrix} x \\ y \end{pmatrix} = \underbrace{\begin{pmatrix} \cos\theta_i & -\sin\theta_i \\ \sin\theta_i & \cos\theta_i \end{pmatrix} \begin{pmatrix} x_i \\ y_i \end{pmatrix}}_{\text{rotation}} + \underbrace{\begin{pmatrix} \delta_{x_i} \\ \delta_{y_i} \end{pmatrix}}_{\text{translation}} \tag{13}$$

In order to take into account the interaction between the ith diffracted acoustic field Φ_{d}^{i}(generated by the ith cavity) and the diffracted acoustic fields generated by the neighboring cavities (jth cavities) Φ_{d}^{j}, we also express the coordinates of the jth local frame in terms of the ith local frame coordinates. The relationships between this two coordinates systems are given by:

$$x_j = \cos(\theta_{ij})\, x_i - \sin(\theta_{ij})\, y_i + \delta_{x_{ij}} \cos\theta_j + \delta_{y_{ij}} \sin\theta_j \tag{14}$$

$$y_j = \sin(\theta_{ij})\, x_i + \cos(\theta_{ij})\, y_i - \delta_{x_{ij}} \sin\theta_j + \delta_{y_{ij}} \cos\theta_j \tag{15}$$

where:

$$\theta_{ij} = \theta_i - \theta_j \tag{16}$$

$$\delta_{x_{ij}} = \delta_{x_i} - \delta_{x_j} \tag{17}$$

$$\delta_{y_{ij}} = \delta_{y_i} - \delta_{y_j} \tag{18}$$

θ_j is the angle between the jth local frame and the reference frame. θ_{ij} is the angle between the local frames i and j. $(\delta_{x_i}, \delta_{y_i})$ and $(\delta_{x_j}, \delta_{y_j})$ are the

coordinates for the local frames i and j centers respectively in the reference frame (O, x, y). $\delta_{x_{ij}}$ and $\delta_{y_{ij}}$ are the distances between the frames i and j centers along the x and y axes respectively.

The relationships (13)-(15) allows uniforming the coordinates system. Indeed, we express all the coordinates as function of the ith local frame coordinate system (x_i and y_i). Then, we carry out the same procedure used in [8]: we expand the trigonometric functions depending on ξ_i and η_i in equation (10) in terms of Jacobi's polynomials, $G^{(2,\frac{3}{2})}(x)$ for the sine function and $G^{(1,\frac{1}{2})}(x)$ for the cosine function, to apply the orthogonality relationships between the same polynomials. Equations (11) and (12) are projected into the functional space defined by the trigonomeric functions. The combination of the $3 \times N$ boundary conditions allows obtaining a system of matrix equation given by the relationships (19)-(22) depending on the angles θ_i and θ_j between the ith and the jth local frames and the reference frame respectively:

$$[A^i_{mn}][G^{0,0}_{m,n,s,t}] + \sum_{j\neq i}\sum_{\mu_j=0}^{1}\sum_{\nu_j=0}^{1}[M^{j,\mu_j,\nu_j}_{mn}][GC^{0,0,\mu_j,\nu_j}_{m,n,s,t}] = [\Lambda^{0,0,\theta_i}_{s,t}],\ 1 \leq i \leq N \tag{19}$$

$$[B^i_{mn}][G^{0,1}_{m,n,s,t}] + \sum_{j\neq i}\sum_{\mu_j=0}^{1}\sum_{\nu_j=0}^{1}[M^{j,\mu_j,\nu_j}_{mn}][GC^{0,1,\mu_j,\nu_j}_{m,n,s,t}] = [\Lambda^{0,1,\theta_i}_{s,t}],\ 1 \leq i \leq N \tag{20}$$

$$[C^i_{mn}][G^{1,0}_{m,n,s,t}] + \sum_{j\neq i}\sum_{\mu_j=0}^{1}\sum_{\nu_j=0}^{1}[M^{j,\mu_j,\nu_j}_{mn}][GC^{1,0,\mu_j,\nu_j}_{m,n,s,t}] = [\Lambda^{1,0,\theta_i}_{s,t}],\ 1 \leq i \leq N \tag{21}$$

$$[D^i_{mn}][G^{1,1}_{m,n,s,t}] + \sum_{j\neq i}\sum_{\mu_j=0}^{1}\sum_{\nu_j=0}^{1}[M^{j,\mu_j,\nu_j}_{mn}][GC^{1,1,\mu_j,\nu_j}_{m,n,s,t}] = [\Lambda^{1,1,\theta_i}_{s,t}],\ 1 \leq i \leq N \tag{22}$$

where A^i_{mn}, B^i_{mn}, C^i_{mn}, and D^i_{mn} are the unknown amplitudes of the acoustic diffracted field Φ^i_{d} sought.

$$M_{mn}^{j,\mu_j,\nu_j} = \begin{cases} A_{mn}^j \text{ if } (\mu_j,\nu_j) = (0,0) \\ B_{mn}^j \text{ if } (\mu_j,\nu_j) = (0,1) \\ C_{mn}^j \text{ if } (\mu_j,\nu_j) = (1,0) \\ D_{mn}^j \text{ if } (\mu_j,\nu_j) = (1,1) \end{cases} \tag{23}$$

$$\begin{aligned} G_{m,n,s,t}^{\mu_i,\nu_i} &= \iint_{\mathbb{R}_+^2} \frac{J_{2m+\mu_i}(\alpha) J_{2s+1+\mu_i}(\alpha) J_{2n+\nu_i}(\beta) J_{2t+1+\nu_i}(\beta)}{\alpha\beta\sqrt{\alpha^2 + (\frac{a_i}{b_i}\beta)^2 - (ka_i)^2}} \,\mathrm{d}\alpha\,\mathrm{d}\beta \\ &- \sum_{p,q\geq 0} \left(\frac{\pi^2}{\epsilon_{2p+\mu_i}\epsilon_{2q+\nu_i}\gamma_{2p+\mu_i,2q+\nu_i}} \frac{\Gamma_{2p+\mu_i,2q+\nu_i}^{+i}}{\Gamma_{2p+\mu_i,2q+\nu_i}^{-i}} \frac{J_{2m+\mu_i}\left(\frac{2p+\mu_i}{2}\pi\right) J_{2s+1+\mu_i}\left(\frac{2p+\mu_i}{2}\pi\right)}{\frac{2p+\mu_i}{2}\pi} \right. \\ &\left. \times \frac{J_{2n+\nu_i}\left(\frac{2q+\nu_i}{2}\pi\right) J_{2t+1+\nu_i}\left(\frac{2q+\nu_i}{2}\pi\right)}{\frac{2q+\nu_i}{2}\pi} \right) \end{aligned} \tag{24}$$

$$\begin{aligned} \Lambda_{s,t}^{\mu_i,\nu_i,\theta_i} &= -2\mathrm{j}^{\mu_i+\nu_i} A \frac{J_{2s+1+\mu_i}\left(a_i\left(k_x\cos\theta_i + k_y\sin\theta_i\right)\right)}{a_i\left(k_x\cos\theta_i + k_y\sin\theta_i\right)} \\ &\times \frac{J_{2t+1+\nu_i}\left(b_i\left(-k_x\sin\theta_i + k_y\cos\theta_i\right)\right)}{b_i\left(-k_1\sin\theta_i + k_2\cos\theta_i\right)} e^{-\mathrm{j}k_x\delta_{x_i}} e^{-\mathrm{j}k_y\delta_{y_i}} \end{aligned} \tag{25}$$

$$\begin{aligned} GC_{m,n,s,t}^{\mu_i,\nu_i,\mu_j,\nu_j} &= (-1)^{\mu_j+\nu_j} \iint_{\mathbb{R}_+^2} \frac{J_{2m+\mu_j}(\alpha) J_{2m+\nu_j}(\alpha)}{2} \\ &\times \left[\left(\frac{J_{2s+1+\mu_i}\left(\ell_1(\alpha,\beta)\right)}{\ell_1(\alpha,\beta)} \frac{J_{2t+1+\nu_i}\left(\ell_2(\alpha,\beta)\right)}{\ell_2(\alpha,\beta)} + \frac{J_{2s+1+\mu_i}\left(\ell_3(\alpha,\beta)\right)}{\ell_3(\alpha,\beta)} \frac{J_{2t+1+\nu_i}\left(\ell_4(\alpha,\beta)\right)}{\ell_4(\alpha,\beta)} \right) \right. \\ &\times \cos\left(\Delta_x\alpha + (\mu_i+\mu_j)\frac{\pi}{2}\right) \cos\left(\Delta_y\beta + (\nu_i+\nu_j)\frac{\pi}{2}\right) \\ &+ \left(-\frac{J_{2s+1+\mu_i}\left(\ell_1(\alpha,\beta)\right)}{\ell_1(\alpha,\beta)} \frac{J_{2t+1+\nu_i}\left(\ell_2(\alpha,\beta)\right)}{\ell_2(\alpha,\beta)} + \frac{J_{2s+1+\mu_i}\left(\ell_3(\alpha,\beta)\right)}{\ell_3(\alpha,\beta)} \frac{J_{2t+1+\nu_i}\left(\ell_4(\alpha,\beta)\right)}{\ell_4(\alpha,\beta)} \right) \\ &\left. \times \sin\left(\Delta_x\alpha + (\mu_i+\mu_j)\frac{\pi}{2}\right) \sin\left(\Delta_y\beta + (\nu_i+\nu_j)\frac{\pi}{2}\right) \right] \mathrm{d}\alpha\,\mathrm{d}\beta,\ 1 \leq i \leq N \end{aligned} \tag{26}$$

with:

$$\ell_1(\alpha,\beta) = \frac{a_i}{a_j}\cos(\theta_i-\theta_j)\alpha + \frac{a_i}{b_j}\sin(\theta_i-\theta_j)\beta \tag{27}$$

$$\ell_2(\alpha,\beta) = \frac{b_i}{b_j}\cos(\theta_i-\theta_j)\beta + \frac{b_i}{a_j}\sin(\theta_i-\theta_j)\alpha \tag{28}$$

$$\ell_3(\alpha,\beta) = \frac{a_i}{a_j}\cos(\theta_i-\theta_j)\alpha - \frac{a_i}{b_j}\sin(\theta_i-\theta_j)\beta \tag{29}$$

$$\ell_4(\alpha,\beta) = \frac{b_i}{b_j}\cos(\theta_i-\theta_j)\beta - \frac{b_i}{a_j}\sin(\theta_i-\theta_j)\alpha \tag{30}$$

$$\Delta_x = \frac{\delta_{x_{ij}}}{a_j}\cos\theta_j + \frac{\delta_{y_{ij}}}{a_j}\sin\theta_j \tag{31}$$

$$\Delta_y = \frac{\delta_{y_{ij}}}{b_j}\cos\theta_j - \frac{\delta_{x_{ij}}}{b_j}\sin\theta_j \tag{32}$$

$$\Gamma_{p,q}^{\pm i} = 1 \pm \frac{\gamma_{pq}^i + \mathrm{j}ka_i\eta_{\mathrm{ad}}^i}{\gamma_{pq}^i - \mathrm{j}ka_i\eta_{\mathrm{ad}}^i} e^{2\gamma_{pq}^i d_i} \tag{33}$$

$$\epsilon_p = \begin{cases} 2 \text{ if } p = 0 \\ 1 \text{ else} \end{cases} \tag{34}$$

The functions $G_{m,n,s,t}^{\mu_i,\nu_i}$ and $\Lambda_{s,t}^{\mu_i,\nu_i,\theta_i}$ defining the solution of the non-coupled problem are independent from the angles between the local frames $(\theta_i - \theta_j)$. Indeed, in the case of the non-coupled solution, the interaction between acoustic diffracted fields is considered void, each cavity sound radiating independently.

The $4 \times N$ unknown amplitudes A_{mn}^i, B_{mn}^i, C_{mn}^i and D_{mn}^i are obtained by inverting the system of matrix equations, given by relationships (19)-(22). It is difficult to use direct method (LU decomposition, Gauss-Jordan elimination, etc.) due to the obtained system of equations complexity. Thus, we use the Gauss-Seidel method. This method is an iterative technique. In order to accelerate the convergence to the coupled problem solution, we chose the solution of the non-coupled problem as an initial value [8].

3. Principle of finite element modeling

We chose to compare our model to the finite element modelling (FEM) method before experiment. The simulation was performed by Comsol 4.0 software. The tested gratings will be presented in details in the section 4.

FEM involves subdividing the studied structure containing the cavities into two sections. The first section was a steel plate containing the rectangular cavities, characterized by density $\rho = 7850\,\mathrm{Kg\,m^{-3}}$ and sound velocity $v = 6400\,\mathrm{m\,s^{-1}}$. The choice of steel ensures a very high acoustic reflection ($R = 1$) at the borders as considered in the theoretical model. The second section was the propagation element which is the air. The studied structure was insonified by a fixed frequency spherical wave. The periphery of these two sections was coated by Perfectly Matched Layers (PML) in order to simulate free field condition [10]. This features are shown in the figure 3. The PLM size was 5 cm since the width determines the longest wavelength that can be supported by the layer [12]. Tetrahedral elements was used to mesh the geometry. The total number of elements was 165843.

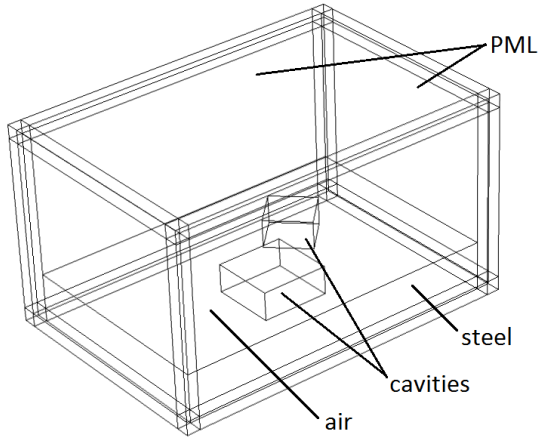

Figure 3: Principle of finite element modeling.

4. Results and discussion

To validate the model, the sound pressure profiles were measured at 20 cm above two studied gratings in the x direction as indicated in the figure 4(a) and 4(b) respectively

- a periodic array of three $(0.50 \times 0.48 \times 0.21)\,\mathrm{m^3}$ rigid cavities. The periodic spacement was 2 cm along the x axis. The reference frame was centered on the central cavity. The spherical source was placed 1 m above the central cavity (see figure 4(a)). This array was studied

in order to check the validity of the model in the case of a grating of parallel rectangular cavities.

- an aperiodic grating of two non parallel rigid cavities. The size of the first cavity was $(0.50 \times 0.48 \times 0.21)\,\mathrm{m}^3$. It was centered on the reference frame. The size of the second cavity was $(0.35 \times 0.34 \times 0.21)\,\mathrm{m}^3$. It was rotated by an angle of $\theta_i = 45°$. The coordinates of the center of its local frame was $(0.56, 0.50)_{(O,x,y)}\,\mathrm{m}$. The spherical source was placed 1.02 m above the first cavity (see figure 4(b)).

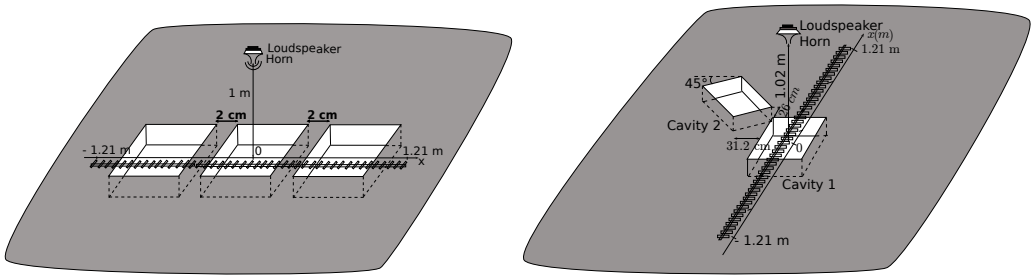

(a) (b)

Figure 4: Geometry of the two studied gratings : the array of the three periodic cavities (a) and the grating of the two non-parallel cavities (b)

The bottom of the cavities was considered infinitely rigid (steel that $\eta_{\mathrm{ad}} = 0$). The profiles were formed by tiled polystyrene blocks to ensure a high acoustic reflection coefficient. The measurements were taken in free-field conditions in the Institut national de recherche et de securite (INRS) semi-anechoic chamber. The sound source used for the test was a horn with a $15\,mm$ outlet diameter [8]. A 10 cm diameter Pioneer TS E1077 loudspeaker was fixed between the horn and the cylindrical body. Such a source allowed the emission of spherical waves in the frequency range of interest $[100 - 5000\,\mathrm{Hz}]$. The sound pressure profiles were measured by 45 sensors along the x-axis. Measurement was performed in three stages for three juxtaposed positions of an antenna fitted with 15 microphones ($1/4$ inch) placed 0.2 m above the wall facings studied. These were spaced at 5.5 cm intervals and their positions were chosen such that the central microphone of the 45-sensor virtual array was positioned directly below the loudspeaker.

The developed model is valid for plane waves. In oder to be comparable with experiment, the spherical incident acoustic wave was decomposed into

plane waves. Thus, the theoretical total diffracted field was obtained by summing all the diffracted fields generated by the respective plane waves [8].

All the acoustic pressure profiles are normalized with respect to the signal of the central microphone ($x = 0$). This normalization allows easy comparison of numerical and experimental results independently of the real source power.

Figures 5 and 6 show a comparison between our model, the finite element modeling (FEM) method and experiment for different frequencies. A good agreement between the theoretical and experimental results was obtained confirming the validity of the model for parallel and non-parallel gratings. The curves become more irregular as frequency increases. This phenomenon is due to more directive scattering at these frequencies. In figure 6 and above 500 Hz, the curves become more symmetric. The diffracted sound field generated by the second cavity has less ability to disrupt the diffracted field generated by the first cavity at high frequencies. The distance between the two cavities becomes important compared to the wavelength at high frequencies.

The differences between the FEM method and our model are mostly situated in the extremities of the normalized pressure profiles. These differences are probably due to non-perfect PML boundary condition (anechoic termination conditions) in the case of the FEM method [11]. However, the comparison between our model and the FEM method confirms the accuracy of our method.

Frequency (Hz)	230	780	1000	1600
Convergence order S	2	3	5	5
Calculation time (mn)	2	15	40	80

Table 1: Calculation time and convergence order S for the different frequencies presented in the grating of the three parallel rectangular cavities case

Frequency (Hz)	300	500	780	1900
Convergence order S	2	2	3	5
Calculation time (mn)	2	3	12	120

Table 2: Calculation time and convergence order S for the different frequencies presented in the grating of the two non parallel rectangular cavities case

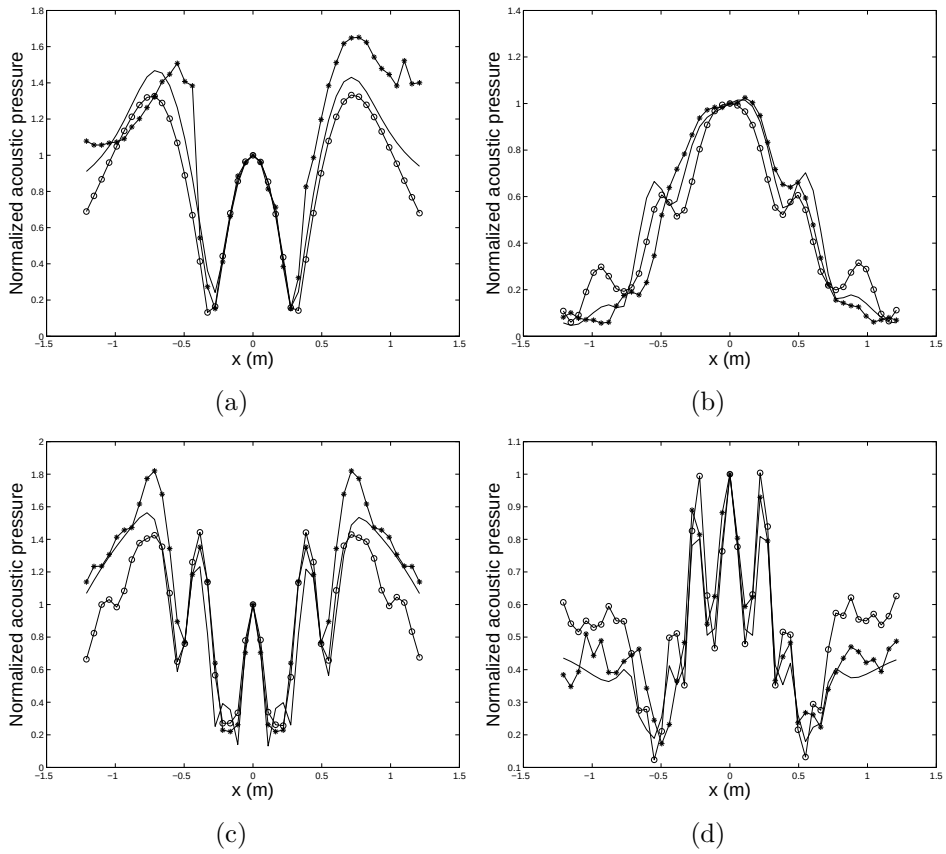

Figure 5: Normalized acoustic pressure $0,2\,m$ above the periodic array of the three parallel rectangular cavities for different frequencies: 230 Hz (a), 780 Hz (b), 1000 Hz (c) and 1600 Hz (d). Model (——), FEM (—o—), Experiment (—∗—).

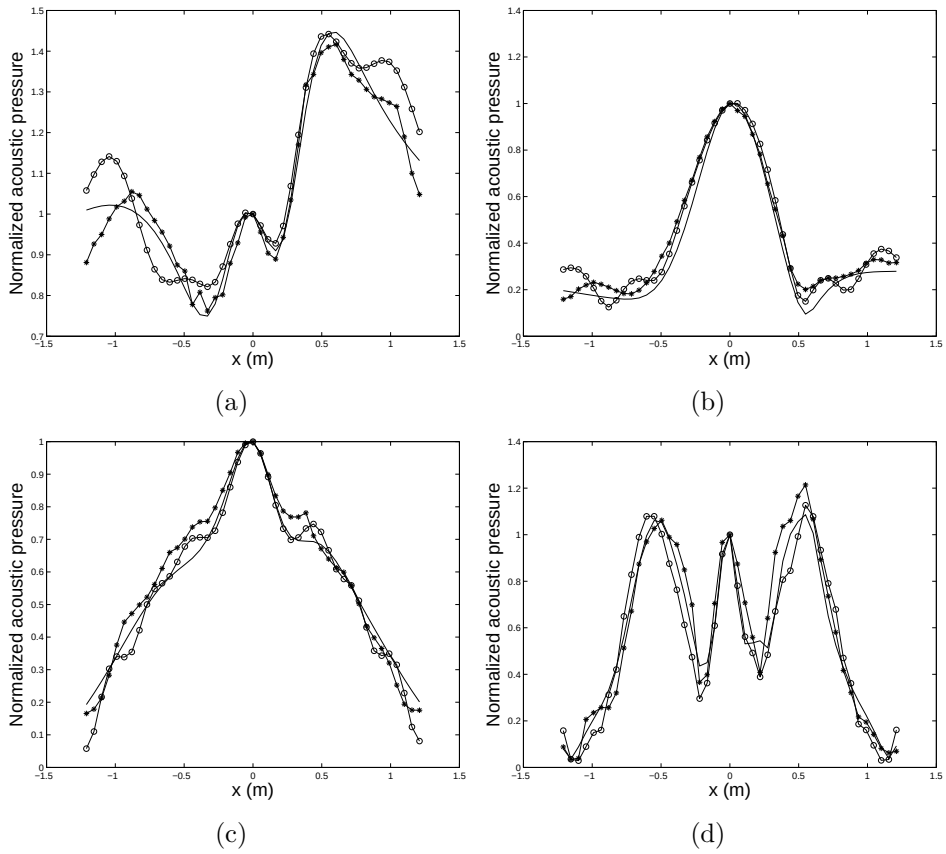

Figure 6: Normalized acoustic pressure $0,2\,\mathrm{m}$ above the grating of the two non parallel rectangular cavities for different frequencies: 300 Hz (a), 500 Hz (b), 780 Hz (c) and 1900 Hz (d). Model (——), FEM (—o—), Experiment (—∗—).

Several simulations allowed us to determine the optimal order of convergence for each frequency. For example, figure 7 shows the variation of the total acoustic velocity with respect of the position x for the frequency 300 Hz in the case of the grating of two non parallel rectangular cavities for different order S. The curves obtained for $S = 2$ and $S = 3$ are superimposed. We conclude that the convergence is obtained for an order $S = 2$ for the frequency 300 Hz. The same procedure was applied for the other frequencies.

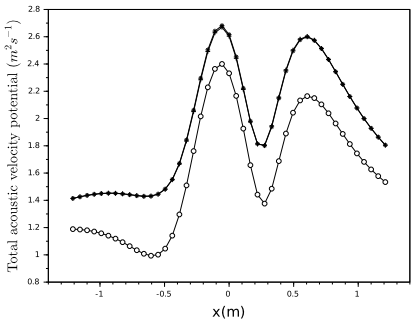

Figure 7: Total acoustic velocity for different order S in the case of the grating of two non parallel rectangular cavities for 300 Hz. $S = 1$ (—o—), $S = 2$ (—∗—), $S = 1$ (—+—)

The convergence order S and the calculation time of the different theoretical results of the two studied gratings are given in tables 1 and 2. All the computations were made on a Personal Computer with a 3.07 GHz intel Xeon processor and a 8 Gb of random access memory. The calculation time increases as the frequency and the convergence order S increase. Indeed, the bigger the size of the matrices is, the slower the inversion of the system of matrix equations (19)-(22) is. The calculation time will could be faster if the spherical source had been taken directly as the incident wave in our model. Indeed, in our computation we decompose the spherical acoustic wave into a finite number of acoustic plane waves. Then we calculate the total scattered acoustic field by summing all the obtained elementary scattered fields. The calculation of the FEM was made simultaneously for all the four frequencies for each grating. The calculation time was 150 mn for the four presented frequencies for each grating.

In order to study the coupling phenomena between cavities with respect to frequency and spacing, we compare the coupled solution and the uncou-

pled solution for four periodic arrays of three $(0.50 \times 0.48 \times 0.21)\,\mathrm{m}^3$ rigid same cavities. The four arrays differs in spacing e between the cavities: $e = 0.02\,\mathrm{m}$, $e = 0.07\,\mathrm{m}$, $e = 0.12\,\mathrm{m}$ and $e = 0.34\,\mathrm{m}$. Figure 8 shows a comparison between the values of RMSE parameter [8] obtained for the coupled solution and the uncoupled solution for the four different spacings. These curves show that the convergence of the coupled solution and the uncoupled solution is obtained more rapidly when the spacing between the cavities is more important. Table 3 shows the different convergence frequencies of the coupled and the uncoupled solution for the four studied spacings. In the case of the nearest cavities ($e = 0.02\,\mathrm{m}$) this convergence is obtained for 930 Hz. However, for the more distant cavities ($e = 0.34\,\mathrm{m}$), the convergence is obtained for 500 Hz. Accordingly, the convergence between the model coupled and uncoupled model is obtained from 930 Hz for all spacings considered. It is therefore possible to save calculation time by neglecting the coupling phenomena between cavities from this frequency. This limit is valid only for this studied configuration. This study confirms that the coupling depends on the spacing between cavities and frequency. The coupling becomes weak when the wavelength become small compared to the spacing between cavities. The convergence frequency is the minimum frequency from which the difference of the coupled and the uncoupled RMSE values is close to zero for all the frequencies above.

Spacing	Convergence frequency
0.02 m	930 Hz
0.07 m	780 Hz
0.12 m	580 Hz
0.34 m	500 Hz

Table 3: Convergence frequencies of the coupled and the uncoupled solutions for the four studied spacings.

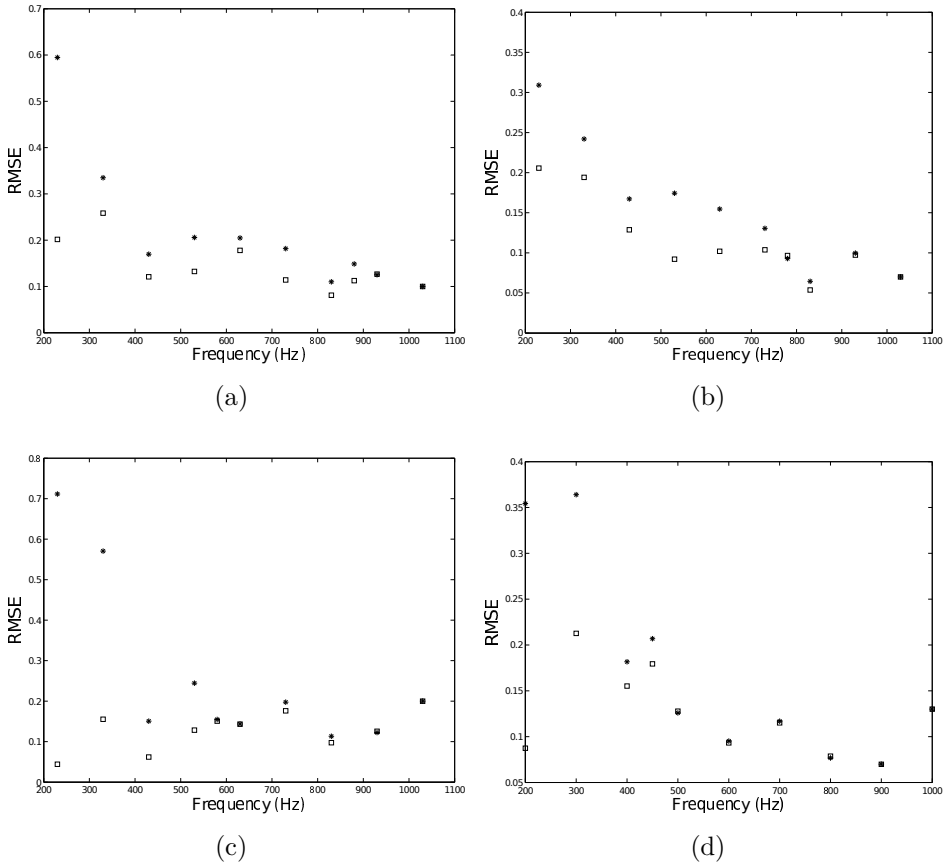

Figure 8: Comparison of the RMSE parameter value obtained for the coupled solution and the uncoupled solution for the four periodic arrays of three $(0.50 \times 0.48 \times 0.21)\,\mathrm{m}^3$ rigid same cavities studied: 0.02 m (a), 0.07 m (b), 0.12 m (c) and 0.34 m (d). Coupled solution ($\square$), Non coupled solution ($*$).

5. Conclusion

A generalization of the model proposed in [8] to the case of gratings of non parallel rectangular cavities of different size and spacing was performed using the Kobayashi Potential method. A comparison between the analytical model, the FEM model and experiment was performed for a grating of two non parallel rectangular cavities and a periodic array of three rectangular cavities. A good agreement between the theoretical and experimental results was obtained for different frequencies.

A study of the coupling phenomena between cavities with respect to frequency and spacing was made by comparing the coupled and the uncoupled solutions for four periodic arrays of three $(0.50 \times 0.48 \times 0.21)\,\mathrm{m}^3$ rigid same cavities differing by spacing. This study shows that we can neglect the coupling between cavities from frequencies above 1000 Hz. This limit is valid only for this studied configuration. Thanks to the model, it will be possible to determine the acoustic field above complex wall facings containing parallel and non-parallel rectangular cavities with different size and spacing.

The model allows calculating separately the diffracted sound field above a grating of rectangular cavities. This allows determination of the scattered coefficient for different gratings composed of non parallel rectangular cavities. It can lead also to characterize such a wall facing by an equivalent admittance or an equivalent reflection or absorption coefficient which can simplify the acoustic study of confined spaces delimited by this kind of wall facings containing rectangular cavities. This will be the purpose of a future work.

[1] R. L. Holford, Scattering of sound waves at a periodic, pressure-release surface: An exact solution, The Journal of the Acoustical Society of America 70 (4) (1981) 1116 – 1128.

[2] A. De Bruijn, The Sound Absorption of an Absorbing Periodically Uneven Surface of Rectangular Profile, Acustica 18 (1967) 123 – 131.

[3] Y. Ando, K. Kato, Calculations on the Sound Reflection from Periodically Uneven Surfaces of Arbitrary Profile, Acustica 35 (1976) 322 – 329.

[4] J. Ducourneau, L. Bos, V. Planeau, A. Faiz, S. S. Lami, A. Nejade, Prediction of the acoustic pressure above periodically uneven facings in industrial workplaces, Journal of Sound and Vibration 329 (11) (2010) 2276 – 2290.

[5] H. H. Park, H. J. Eom, Electromagnetic scattering from multiple rectangular apertures in a thick conducting screen, IEEE Transactions on Antennas and Propagation 47 (6) (1999) 1056–1060.

[6] K. Hongo, N. Furusawa, H. Horis, Two-dimensional multiple scattering for n slit array, Electronics and Communications in Japan (Part I: Communications) 63 (5) (1980) 89 – 96.

[7] K. Hongo, Radiation characteristics of flanged parallel-plate waveguide arrays, Trans. Inst. Electronics and Communications Engineering in Japan 61-B (1978) 161 – 165.

[8] A. Khanfir, A. Faiz, J. Ducourneau, J. Chatillon, S. S. Lami, Scattered acoustic field above a grating of parallel rectangular cavities, Journal of Sound and Vibration 332 (4) (2013) 1047 – 1060.

[9] A. M. Ondet and J. L. Barbry, Modeling of sound propagation in fitted workshops using ray tracing, The Journal of the Acoustical Society of America 85 (2) (1989) 787–796.

[10] N. Gonzlez-Salido, A. Islas-Cital, F. Camarena, R. Pico, and P. R. Atkins, Scattering of complex geometries by Finite Element Method, In Proceedings of the Acoustics 2012 Nantes Conference, Nantes, France, April 2012.

[11] N. Li, C. H. Zhai and L. L. Xie, The PML and MTF method based on hybrid finite element method: a comparative study, In Proceedings of the 14th World Conference on Earthquake Engineering , Beijing, China, October 2008.

[12] K. Duru and G. Kreiss, Numerical interaction of boundary waves with perfectly matched layers in two space dimensional elastic waveguides, Wave Motion 51 (3) (2014) 445–465.